Characterization and thermal behavior of hydroxyapatite prepared by precipitation.

Lenka Šimková[1], Petra Šulcová[1]

[1]*The University of Pardubice, Faculty of Chemical Technology, Department of Inorganic Technology, Studentská 95, 532 10 Pardubice, Czech Republic*

E-mail: lenka.simkova1@student.upce.cz; petra.sulcova@upce.cz

Abstract

The aim of this study was to find appropriate precipitation conditions (Ca/P ratio, pH and precipitation rate) for the synthesis of hydroxyapatite (HAP; $Ca_{10}(PO_4)_6(OH)_2$) and to determine the effect of precipitation conditions on its thermal behavior. Hydroxyapatite was synthesized by precipitation. Three ratios of Ca/P (1; 1.67; 3) were selected for the synthesis, then pH 7 and 12 was selected and the ammonium dihydrogen phosphate precipitation rate was set to 2 ml/min. The prepared powders were studied from the standpoint of particle size distribution, crystal size and morphology (optical microscope, scanning electron microscope), phase composition (X-ray diffraction analysis) and thermal stability in relation to the Ca/P ratio.

Keywords

Hydroxyapatite, precipitation, Ca/P ratio, XRD, SEM, Simultaneous DTA-TG analysis

Acknowledgments

Introduction

The term "apatite" applies to a group of compounds with a general formula in form $M_{10}(XO_4)_6Z_2$, where Z- may be typically OH^-, F^-, Cl^- [1]. Hydroxyapatite (HAP) has the molecular structure of apatite, where M is calcium (Ca^{2+}), X is phosphorus (P^{5+}) and Z is the hydroxyl group (OH^-). This composition of elements is known as stoichiometric hydroxyapatite and its atomic ratio Ca/P is 1.67. The chemical formula of HAP is $Ca_{10}(PO_4)_6(OH)_2$, with 39.89 % by weight of calcium, 18.50 % of phosphorus, 41.41 % of oxygen and 0.20 % of hydrogen [2, 3].

The reason for the extension of phosphate pigments is strict environmental and hygienic limits, which require the replacement of toxic lead and chromate pigments with nontoxic but very effective pigments [4]. Hydroxyapatite [$Ca_{10}(PO_4)_6(OH)_2$, HAP] is a stable apatite compound and has been used widely due to its similarity to human bone composition, bioactivity, and biocompatibility [5]. Consequently, HAP was easily considered as a bioactive material for synthetic bone replacement due to its biocompatibility, and chemical and biological affinity with bone tissue [6].

Synthetic HAP is used as a biomaterial for dental and orthopedic replacements [7]. Apart from medical applications, it has been also applied in the field of heterogeneous catalysis as a promotion because of its bifunctionality, hydrophilic properties and high structural stability [8]. HAP can also be used in other fields, such as wastewater treatment, detection of heavy metals in water [9, 10], electrochemical applications [11] and environmental pollution control [12]. The major applications of hydroxyapatite are its use as a coating of metallic prostheses, which has two significant functions: to protect the implant against corrosion and to improve implant's

biocompatibility with the human body [13]. Since hydroxyapatite is dearly useful for the protection of implants against corrosion it can be functional even for steel protection equal do other phosphate pigments [14].

The most common form of HAP is the hexagonal crystal structure, $P6_3/m$ space group, with Ca/P ratio 1.67 [15]. Stoichiometry, pH, temperature, and rate of reagent addition influence the precipitation of HAP. Therefore, it is crucial to control these aspects to produce HAP with an optimum morphology and crystallinity [16]. The optimum Ca/P molar ratio must be 1.667. However one of the main problems related to HAP processing is the low stability of HAP at temperatures near to the sintering range, which is attributed to deviations from the ideal Ca/P ratio [17]. In addition, a lot of factors contribute to complicating the image: sample structure, particle size, purity, powders surface condition, and particles aggregation can support undesirable decompositions and phase transitions [18]. In consequence, several compounds can be formed such as oxyapatite (OAP), oxyhydroxyapatite (OHAP), β-tricalcium phosphate (β-TCP), calcium oxide and tetracalcium phosphate (TTCP) [19, 20]. Particularly the formation of β-TCP ($Ca_3(PO_4)_2$) as the most likely phenomenon in the decomposition process highlights the importance of the Ca/P ratio in the control of HAP stability [18].

The objective of this work is the synthesis of hydroxyapatite powders by the precipitation method with different Ca/P ratios, pH and the same rate of precipitation of ammonium dihydrogen phosphate. Three ratios of Ca/P = 1; 1.67 and 3 were selected; two pH values of 7 and 12 were chosen, where ammonia hydroxide solution was used to adjust the pH; and precipitation rate was set to 2ml/min. The synthesized powders were characterized by X-ray diffraction in order to identify the phase composition and crystallinity; the morphology of powders was investigated by scanning electron microscopy (SEM), the dimension of the crystals has been studied by a digital optical microscope (OM); the powders were analyzed for particle size distribution and the thermal behavior of powders was explored by thermal analysis, which allows simultaneous registration of the thermoanalytical curves TG and DTA. For our future purpose of using these powders as anti-corrosion coatings to prevent or deceleration corrosion, we want to achieve specific properties of the samples convenient for this application. In terms of the morphology of particles, it is primarily the needle-like shapes and the smallest crystalline size (related to anticorrosive efficiency), the narrowest range of particle size and the hexagonal crystalline system.


Experimental parts

Materials

$Ca(NO_3)_2 \cdot 4H_2O$ (98%, Lachema, Czech Republic), $(NH_4)H_2PO_4$ (98%, Lachema, Czech Republic), NH_4OH (25%, Penta Chrudim, Czech Republic) were used for wet precipitation method. For the synthesis of hydroxyapatite, solutions of starting materials ($Ca(NO_3)_2 \cdot 4H_2O$, $(NH_4)H_2PO_4$) of 1 mol/l were prepared. The precise concentrations of these solutions were determined using analytical methods [21, 22].

Synthesis of HAP

In order to select suitable synthesis conditions for the formation of hydroxyapatite phase, the thermodynamic stability of the hydroxyapatite $Ca_{10}(PO_4)_6(OH)_2$ in aqueous solution was analyzed and approved in laboratory conditions [23]. Figure 1 shows the predominance area

diagram for the Ca^{2+} - PO_4^{3-} water system at 25 °C. The x-axis demonstrates a pH scale scope from 0 to 14 and the y-axis shows the decimal logarithm of the phosphate ions concentration. From the figure, it is evident that hydroxyapatite is stable in the pH range from 4.8 to 14.
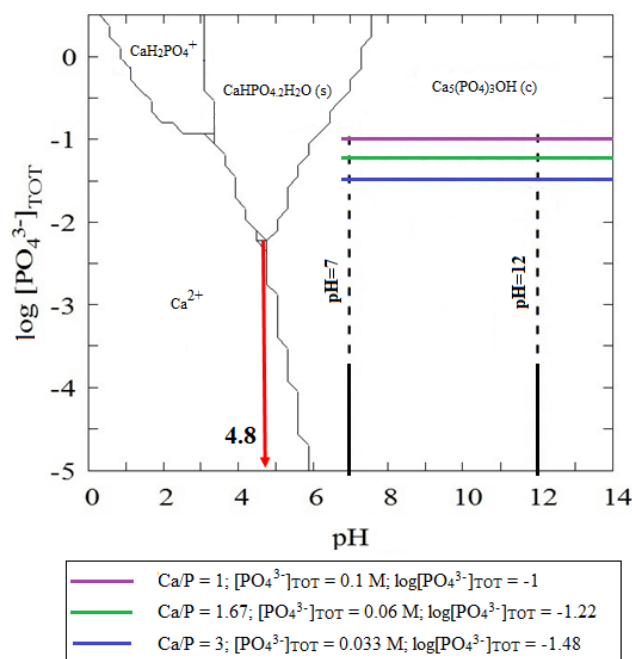
Fig. 1. Predominance area diagram for the Ca^{2+}- PO_4^{3-} system.

Due to this information, three Ca/P ratios were chosen for the synthesis of hydroxyapatite, which were studied at pH = 7 and pH = 12 based on the area of the hydroxyapatite form:
  - Ca/P = 1; in this case, HAP formation occurs in excess of phosphate ions;
  - Ca/P = 1.67; this corresponds to the Ca/P stoichiometry of hydroxyapatite, which is 10/6;
  - Ca/P = 3; HAP formation occurs in excess of calcium ions.

The selected appropriate precipitation conditions (Ca/P=1, 1.67, 3; pH=7, 12) were modified to synthesize pure hydroxyapatite to form $Ca_{10}(PO_4)_6(OH)_2$. For the synthesis of powders, 1M solutions of starting compounds ($Ca(NO_3)_2 \cdot 4H_2O$, $(NH_4)H_2PO_4$) were prepared. Altogether, 4 samples were synthesized at different synthesis conditions (Table 1, precipitation rate of 2 ml/min). The prepared powders were aged during 24 hours, filtered and washed with distilled water to neutral pH, then dried at 80 °C for 6 h. Characterization of the prepared powders was then performed by OM, SEM, XRD and DTA/TG analysis.

Table 1. Overview of the obtained samples and the synthesis conditions

Sample	Composition	Ca/P ratio	pH
1	$Ca_{10}(PO_4)_6(OH)_2$	1	7
2	$Ca_{10}(PO_4)_6(OH)_2$	1.67	7
3	$Ca_{10}(PO_4)_6(OH)_2$	3	7
4	$Ca_{10}(PO_4)_6(OH)_2$	1.67	12

Characterization of HAP

The morphology of the crystals can be measured and characterized by an optical microscope (OM) and scanning electron microscope (SEM). The crystallinity and phase composition of the synthesized powders can be characterized by X-ray diffraction analysis (XRD). Thermal behavior of powders can be described by thermal analysis (DTA/TG).

X-ray diffraction analysis (XRD)

The phase analysis of the powdered materials was studied by X-ray diffraction analysis (XRD). The phase composition was determined using diffractometer MiniFlex 600 (Rigaku, Japan) equipped with a vertical goniometer of 17 cm in the 2θ range of $10°–50°$. The accuracy of goniometer was $\pm0.02°$. X-ray tube with Cu anode (U = 40 kV, I = 15 mA) was used (CuKα radiation). The results were evaluated using the PDF-2 database.

Optical microscope (OM)

The dimension of the crystals was studied by an optical microscope - digital (Dino-Lite Rack, AnMo Electronics, Taiwan) with magnification 10x-70x and 200x.

Particle size distribution (PSD)

The particle size distribution of the powders was measured by equipment Mastersizer 2000/MU (Malvern Instruments, Ltd., UK). This equipment ensures volumetric distribution and uses the laser diffraction on particles dispersed in a liquid medium. The particle size distribution was analyzed by two lasers—red light (He–Ne laser with wavelength 633 nm) and blue light (laser diode with wavelength 466 nm). The pigments were ultrasonically (Bandelin, Germany) homogenized in the solution of $Na_4P_2O_7$ (c = 0.15 mol/dm^3) for 120 s. The signal was evaluated on the basis of Mie scattering. The measurement is taken in three steps, and the results are automatically calculated as average and presented as d_{10}, d_{50}, and d_{90} values.

Scanning electron microscopy (SEM)

The morphology of synthesized powders was studied by scanning electron microscopy (SEM). The resulting image is formed by the secondary signal - reflected or secondary electrons. The morphology of the prepared powder was determined by electron microscope equipped with an IXRF Systems analyzer and a Gresham Sirius 10 detector (Joel Inc., USA).
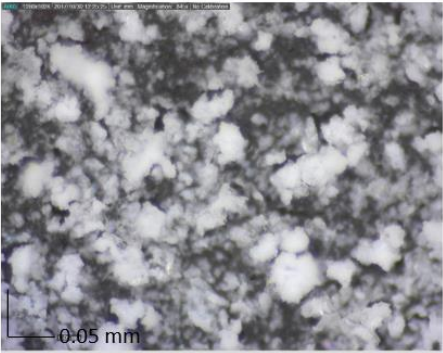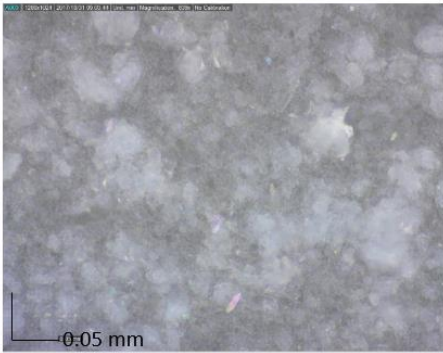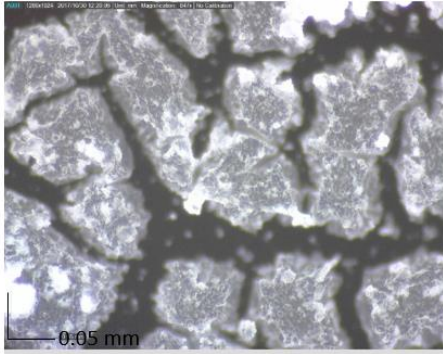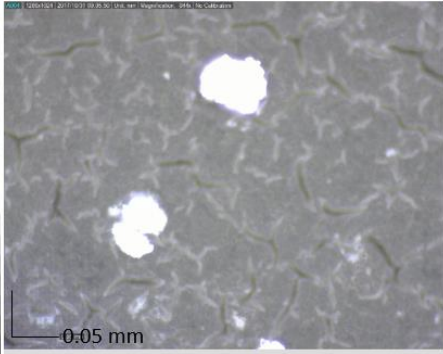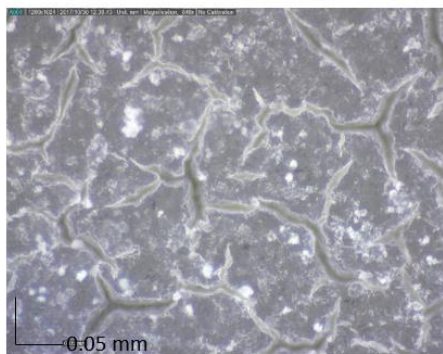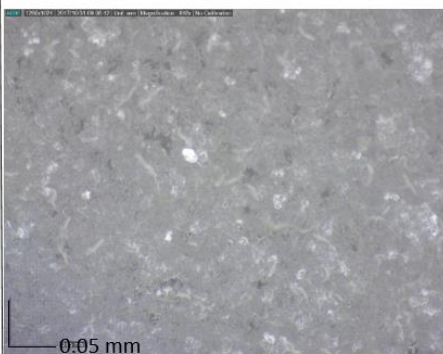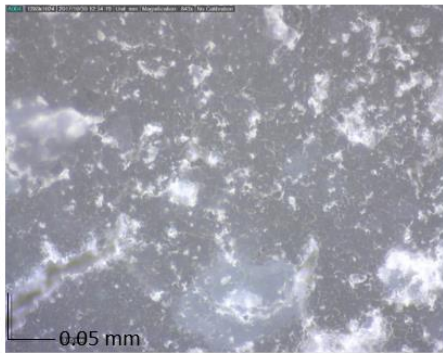
Thermal analysis (DTA/TG)
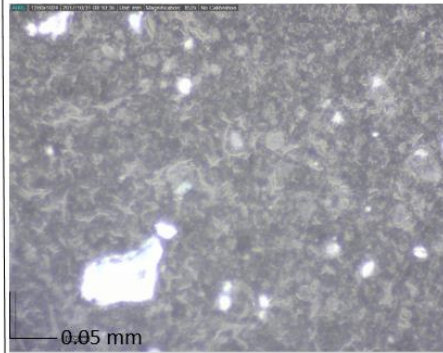
The thermal behavior of studied compounds was followed by simultaneous thermal analysis using the STA 449C Jupiter (NETZSCH, Germany) which allows simultaneous registration of the thermoanalytical curves TG and DTA. The measurements were provided at a temperature interval from 30 to 1100 °C with a heating rate of 10 °C·min^{-1}. The samples were measured in portions approx. 60 mg in corundum crucibles and air atmosphere.

Results and discussion

Optical microscope

In order to observe changes in specimen morphology, samples were measured promptly after precipitation (before aging) and 24 hours after aging. Figure 2 proves the standard appearance of samples (1, 2, 3 and 4) before and after aging. Some samples demonstrated well-shaped

crystals before aging. For all samples after aging, agglomerates of very small crystals were observed, which are visible in Figure 2.

| Standard appearance of samples				
Sample	Ca/P	pH	Before aging	After aging (24 hours)
1	1	7		
2	1.67	7		
3	3	7		
4	1.67	12		

Fig. 2. Standard appearance of measured samples before and after aging (24 hours) using a digital microscope (Dino-Lite Rack - MS34B).

SEM analysis

Measurement by SEM was performed after sample drying and grinding. The measured samples 1, 2, 3 and 4 proved the effect of different Ca/P ratio (samples 1, 2, 3) and pH (samples 2 and 4) on sample morphology.

In order to demonstrate the effect of the Ca/P ratio on the particle shape, samples 1, 2 and 3 were chosen. These samples were prepared at different Ca/P ratios, at the same pH (7) and same precipitation rate (2 ml/min). It was found that the Ca/P ratios have an effect on particle size and shape. Figure 3 shows the comparison of sample 1 (Ca/P = 1, needle-like and tabular shapes) with sample 2 (Ca/P = 1.67, tabular plates) and with sample 3 (Ca/P = 3, needle shapes, bulky formations).

In order to show the effect of pH on the morphology of the particles, samples 2 and 4 (Figure 3) were selected which were synthesized at different pH, the same Ca/P ratio (1.67) and precipitation rate (2 ml/min). Figure 3 proves that the particles of sample 2 (pH = 7) are larger tabular plates, the particles of sample 4 (pH = 12) are bulkier and smaller.
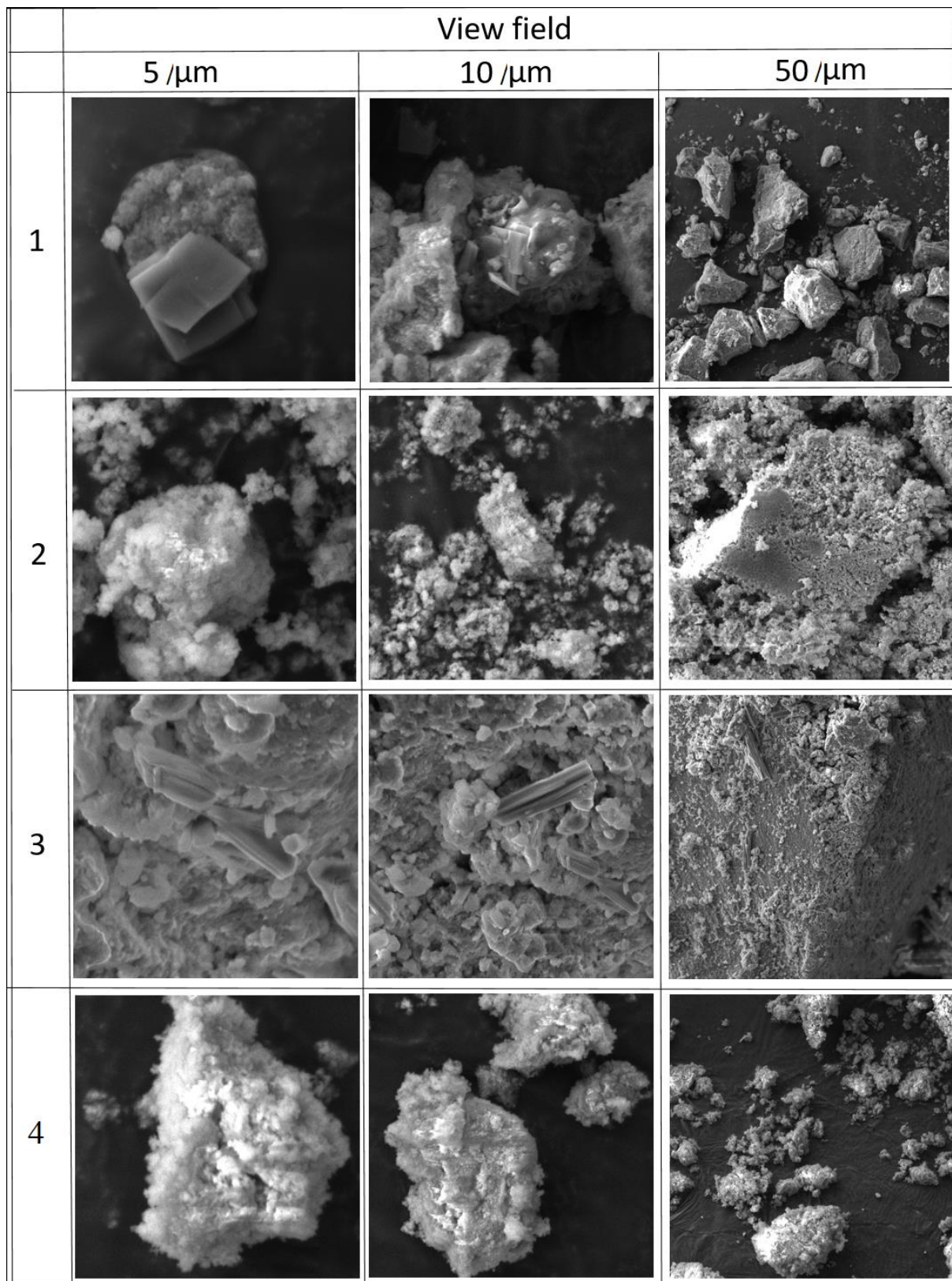
Fig. 3. Comparison of samples 1, 2, 3 and 4 at different view field (5 µm; 10 µm; 50 µm).

Particle size distribution

Particle size distribution of synthesized samples was measured after 24 hours aging with the Mastersizer 2000 MU. Figure 4 shows the distribution curves of all samples (1-4) for illustration. The width of the distribution ranges from 0.4 to 300 μm in particle size range.
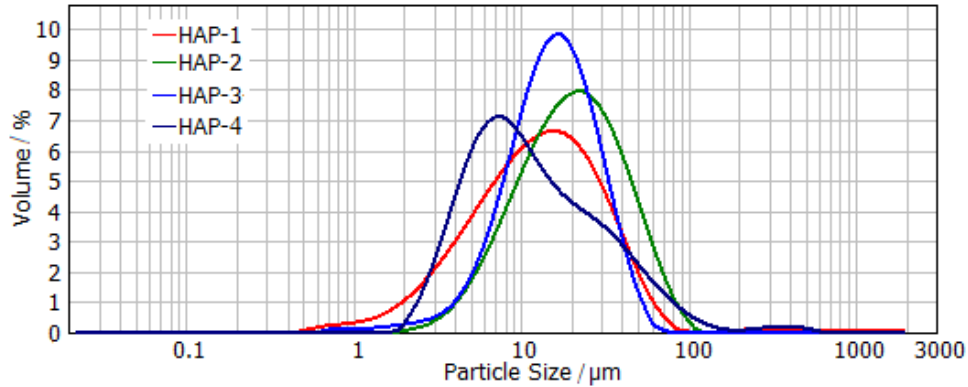
Fig. 4. Distribution curves of all synthesized samples

Table 2 presents the particle size values d_{10}, d_{50}, d_{90} and the distribution span of the measured samples. For measured samples, the d_{10} value is in the range from 3.52 to 7.60 μm, the d_{50} value is from 9.80 to 20.60 μm, the d_{90} value is from 22.43 to 49.60 μm. The distribution range (span) of all analyzed samples is from 1.92 to 3.79. The results indicate the size of the agglomerates and not the real size of the crystals. From the results, it is obvious that sample 1 is characterized by a narrower range of agglomerate size.

**Table 2.** Particle size distribution of all synthesized samples.

Particle size			
Sample	d_{10} /μm	d_{50} /μm	d_{90} /μm	span
1	3.52	9.80	22.43	1.93
2	6.38	13.15	32.37	1.92
3	7.60	20.60	49.60	2.03
4	4.06	10.50	43.87	3.79

XRD analysis

The phase composition of the samples was resolved by XRD analysis. Two distinct structures of hydroxyapatite have been identified: monoclinic and hexagonal. Figure 5 shows the diffractogram of sample 1 containing the hydroxyapatite diffraction line $Ca_{10}(PO_4)_6(OH)_2$ with the parameters: hexagonal crystalline system; space group $P6_3/m$. Figure 2 also demonstrates a diffractogram of sample 2 containing the hydroxyapatite diffraction line $Ca_{10}(PO_4)_6(OH)_2$ with the parameters: monoclinic crystalline system; space group $P2_1/b$. For samples 3 and 4, diffraction lines with the following parameters were identified: hexagonal crystalline system; space group $P6_3/m$. The XRD profiles of both structures are almost identical, it means that both crystalline structures are very similar. For this reason, it is very difficult to properly recognize these structures from the XRD profiles of the measured samples. These structural types of

hydroxyapatite were selected based on the lowest value of FOM (figure of merit), i.e., based on the best match.

**Fig. 5.** Diffractogram of crystal system of hydroxyapatite.
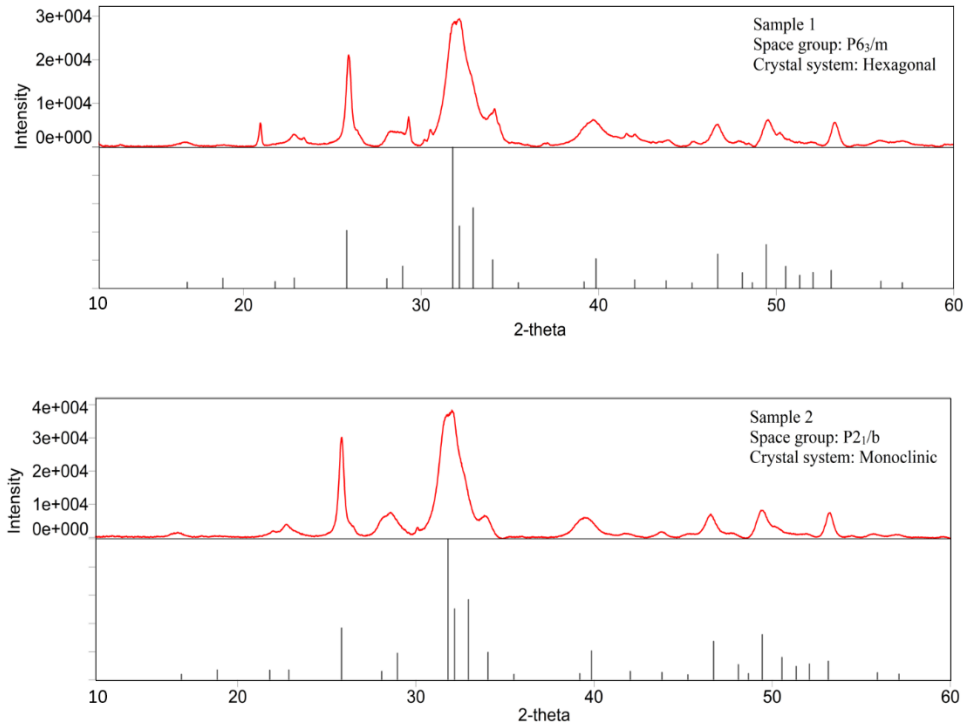
DTA/TG analysis

By DTA/TG analysis, the impact of the Ca/P ratio was proven (Figure 6 and 7, Table 3). There is a consensus that the thermal behavior of HAP occurs in a 4 step process involving dehydroxylation and decomposition:

- Step 1: $Ca_{10}(PO_4)_6(OH)_2 \rightarrow Ca_{10}(PO_4)_6(OH)_{2-2x}O_x\square_x + x\ H_2O$
  (hydroxyapatite)   (oxyhydroxyapatite)
- Step 2: $Ca_{10}(PO_4)_6(OH)_{2-2x}O_x\square_x \rightarrow Ca_{10}(PO_4)_6O + (1-x)\ H_2O$
  (oxyhydroxyapatite)   (oxyapatite)
- Step 3: $Ca_{10}(PO_4)_6O \rightarrow 2\ Ca_3(PO_4)_2$ + $Ca_4(PO_4)_2O$
  (oxyapatite)   (tricalcium phosphate)   (tetracalcium phosphate)
- Step 4: $Ca_4(PO_4)_2O \rightarrow 4\ CaO + P_2O_5 \uparrow$ or $Ca_3(PO_4)_2 \rightarrow 3\ CaO + P_2O_5\uparrow$

Dehydroxylation incorporates the loss of water, which proceeds via the provisional formation of firstly oxyhydroxyapatite (OHAP) and then oxyapatite (OHA) where $\square$ stands for a lattice vacancy in the OH position along the crystallographic c-axis. Decomposition of OHA then proceeds to secondary phases such as tricalcium phosphate (β-TCP) and tetracalcium phosphate (T-TCP). The transformation of HAP has important consequences in bone engineering and plasma coated implants, since β-TCP is a resorbable calcium phosphate, and while it will enhance resorption of HAP implants, decomposition of HAP will also reduce the mechanical properties of the material [24].
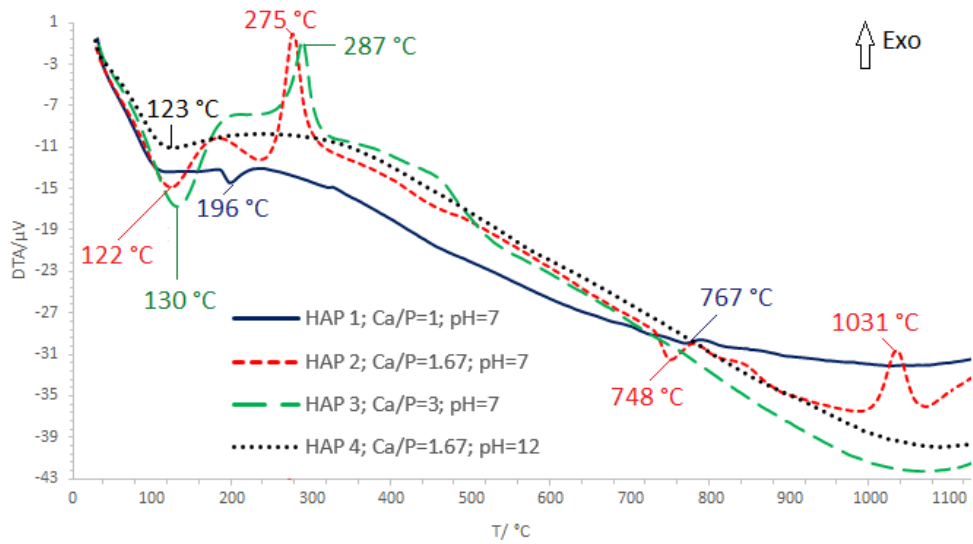
Fig. 6. DTA curves of HAP samples prepared for different Ca/P ratios and pH
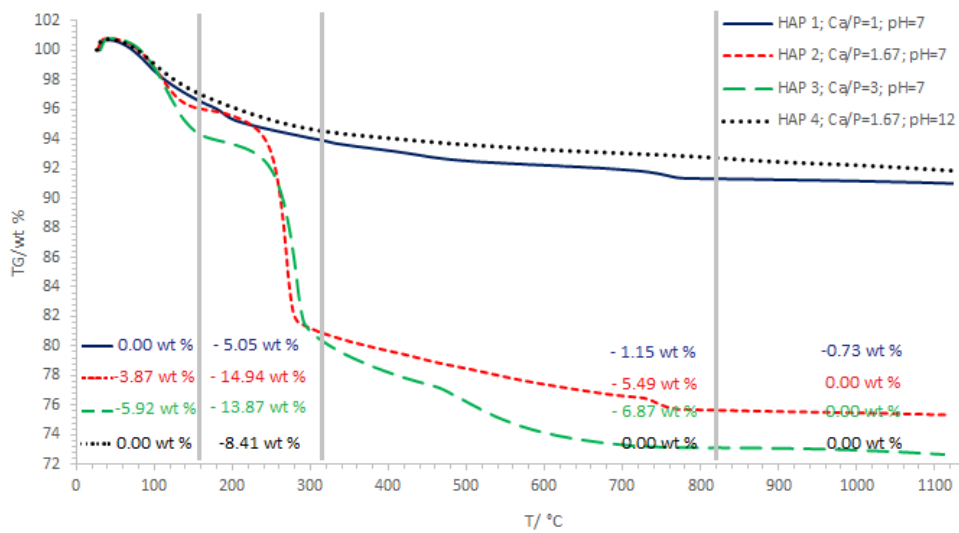
Fig. 7. TG curves of HAP samples prepared for different Ca/P ratios and pH.

Table 3. Overview of processes occurring during hydroxyapatite decomposition

Sample	TA results					Process
	T_{range} /°C	Δm /%	TA effect	T_{peak} /°C	Total Δm /%	
1	80-350	5.05	endo	196	9.15	dehydration
	600-900	1.15	endo	767		dehydroxylation with the formation of OHAP→OHA; OHA decomposes to form β-TCP and T-TCP
2	70-180	3.87	endo	122	24.81	dehydration
	180-500	14.94	exo	275		elimination of ammonia
	550-800	5.49	endo	748		dehydroxylation with the formation of OHAP → OHA; OHA decomposes to form β-TCP and T-TCP
	900-1050	-	exo	1031		decomposition of T-TCP in CaO and $Ca_3(PO_4)_2$
3	80-180	5.92	endo	130	27.65	dehydration
	180-330	13.87	exo	287		elimination of ammonia
	350-800	6.87	-	-		unidentified
4	100-220	-	endo	123	8.41	dehydration

Table 3 provides an overview of the processes that occur during hydroxyapatite decomposing. With decomposition of sample 1, which was prepared at a ratio of Ca/P = 1 and pH = 7, the dehydration of the sample first occurs (196 °C). Subsequently, dehydroxylation occurs to form oxyhydroxyapatite, which is transformed into oxyapatite which decomposes to form β-TCP and T-TCP (767 °C). With decomposition of sample 2, which was synthesized at a ratio of Ca/P = 1.67 and pH = 7, the dehydration of the sample first occurs (122 °C). Then ammonia is eliminated (275 °C). Subsequently, dehydroxylation occurs to form oxyhydroxyapatite, which is transformed into oxyapatite (748 °C). Then the decomposition of oxyapatite follows, which decompose to form β-TCP and T-TCP (748 °C). T-TCP is then spread into CaO and $Ca_3(PO_4)_2$ (1031 °C). With the disintegration of sample 3, which was synthesized at a ratio of Ca/P = 3 and pH = 7, the dehydration of the sample first occurs (130 °C). Subsequently, ammonia is eliminated (287 °C). The last endothermic peak, in the temperature range of 350-800 °C, was not identified. With the decay of sample 4, which was prepared at a ratio of Ca/P = 1.67 and pH = 12, the dehydration of the sample occurs (123 °C). No more peaks in the temperature range of 220-1000 °C were identified.

Conclusion

The selected synthesis conditions (Ca/P ratio = 1, 1.67, 3 and pH = 7, 12) are suitable for the formation of crystalline hydroxyapatite phase. By SEM analysis, the effect of Ca/P ratio and pH on sample particles was proven (different shape and size). Effect of Ca/P ratio on the sample particle morphology: Ca/P = 1 thin needles and plates; Ca/P = 1.67 thin plates; Ca/P = 3 space thin plates. Effect of pH on the sample particle morphology: pH = 7 larger and thin plates; pH = 12 spacer and smaller parts. The phase composition of the samples was determined by XRD analysis, where two distinct hydroxyapatite structures have been identified: hexagonal and

monoclinic. By DTA/TG analysis, the effect of the Ca/P ratio was proven. Thermal behavior of HA occurs in a 4 step process involving dehydroxylation and decomposition. Decomposition of OHA then proceeds to secondary phases such as tricalcium phosphate (β-TCP) and tetracalcium phosphate (T-TCP).

Generally, the best results were obtained in sample 1, which was synthesized at a ratio of Ca/P = 1, the value of pH = 7 and a precipitation rate of 2ml/min. This claim is based on all the analyzes executed, especially with regard to crystallinity (the smallest crystallite size), shape and size of particles (thin needles and tabular plates), particle size distribution (the narrowest range of particle size), hexagonal crystalline system (space group P6$_3$/m) and thermal behavior (produced products β-TCP and T-TCP). By contrast, less suitable precipitation conditions at the Ca/P = 3 ratios were demonstrated (sample 3; bulky formation; the widest range of particle size), and from a thermal behavior aspect, less favorable results at the value of pH = 12 were proved (sample 4, non-expressive peaks).

From the gained results we can confirm that the Ca/P ratio and the value of pH have an effect on the particle morphology as well as its thermal behavior.

References

[1]   Elliott JC. Structure and chemistry of the apatites and other calcium orthophosphates. 2rd. ed. Elsevier; 1994.

[2]   Rivera-Muñoz EM. Hydroxyapatite - based materials: synthesis and characterization. Intech; 2011.

[3]   Friedman H. Complete information guide to rock, minerals and gemstones: The apatite mineral group. Minerals.net: The mineral and gemstone kingdom. http://www.minerals.net/mineral/apatite.aspx. 2014.

[4]   Kalendová A. Technologie nátěrových hmot I, 1st. ed. Univerzita Pardubice; 2003.

[5]   Yang YH, Liu CH, Liang YH, Lin FH, Wu KCW. Hollow mesoporous hydroxyapatite nanoparticles (hmHANPs) with enhanced drug loading and pH-responsive release properties for intracellular drug delivery. J Mater Chem. 2013;1:2447-2450.

[6]   Jarcho M, Bolen CH, Thomas MB, Bobick J, Kay JF, Doremus RH. Hydroxylapatite synthesis and characterization in dense polycrystalline form. J Mater Sci. 1976;11:2027-2035.

[7]   Bellucci D, Sola A, Gazzarri M, Chiellini F, Cannillo V. A new hydroxyapatite-based biocomposite for bone replacement. Mater Sci Eng. 2013;33:1091-1101.

[8]   Gruselle M. Apatites: A new family of catalysts in organic synthesis. J Organomet Chem. 2015;793:93-101.

[9]   Gupta N, Kushwaha AK, Chattopadhyaya MC, Taiwan J. Adsorptive removal of Pb^{2+}, Co^{2+} and Ni^{2+} by hydroxyapatite/chitosan composite from aqueous solution. Inst Chem Eng. 2012;43:125-131.

[10] Salah TA, Mohammad AM, Hassan MA, El-Anadouli BE, Taiwan J. Development of nano-hydroxyapatite/chitosan composite for cadmium ions removal in wastewater treatment. Inst Chem Eng. 2014;45:1571-1577.

[11] Kanchana P, Sekar C. EDTA assisted synthesis of hydroxyapatite nanoparticles for electrochemical sensing of uric acid. Mater Sci Eng. 2014;42:601-607.

[12] Kemiha M, Minh DP, Lyczko N, Nzihou A, Sharrock P. Highly Porous Calcium Hydroxyapatite-based Composites for Air Pollution Control. Procedia Eng. 2014;83:394-402.

[13] Huang Y, Hao M, Nian X. Strontium and copper co-substituted hydroxyapatite-based coatings with improved antibacterial activity and cytocompatibility fabricated by electrodeposition. Ceramics Int. 2016;42:11876-11888.

[14] Gorodylova N, Dohnalová Ž, Šulcová P. Influence of synthesis conditions on physicochemical parameters and corrosion inhibiting activity of strontium pyrophosphates $SrMIIP_2O_7$ (MII = Mg and Zn). Prog Org Coat. 2016;93:77-86.

[15] Meejoo S, Maneeprakorn W, Winotai P. Phase and thermal stability of nanocrystalline hydroxyapatite prepared via microwave heating. Thermochim Acta. 2006;447:115-120.

[16] Kumta PN, Sfeir C, Lee DH, Olton D, Choi D. Nanostructured calcium phosphates for biomedical applications: novel synthesis and characterization. Acta Biomater. 2005;1:65-83.

[17] Wang PE, Chaki TK. Sintering behaviour and mechanical properties of hydroxyapatite and dicalcium phosphate. J Mater Sci-Mater M. 1993;4:150-158.

[18] Tampieri A, Celotti G, Szontagh F, Landi E. Crystallinity in apatites: how can a truly disordered fraction be distinguished from nanosize crystalline domains. J Mater Sci-Mater M. 1997;17:1079-1087.

[19] Savino K, Yates MZ. Thermal stability of electrochemical–hydrothermal hydroxyapatite coatings. Ceram Int. 2015;41:8568-8577.

[20] Sun R, Chen K, Liao Z, Meng N. Controlled synthesis and thermal stability of hydroxyapatite hierarchical microstructures. Mater Res Bull. 2013;48:1143-1147.

[21] Šimková L, Gorodylova N, Dohnalová Ž, Šulcová P. Influence of precipitation conditions on the synthesis of hydroxyapatite. Ceram Silik. 2018;62:1-9.

[22] Harvey D. Modern analytical chemistry. 1st. ed. University of Tennessee; 2008.

[23] Hermassi M, Valderrama C, Dosta J, Cortina JL, Batis NH. Evaluation of hydroxyapatite crystallization in a batch reactor for the valorization of alkaline phosphate concentrates from wastewater treatment plants using calcium chloride. Chem Eng J. 2015;267:142-152.

[24] Chetty AS, Wepener I, Marei MK, Kamary YEl, Moussa R.M. Synthesis, properties, and applications of hydroxyapatite. In: Hydroxyapatite: Synthesis, Properties and Applications. New York: Nova Scie Pub Inc; 2012. pp. 91–133.